Fusion Engineering and Design 192 (2023) 113611

Contents lists available at ScienceDirect

Fusion Engineering and Design

journal homepage: www.elsevier.com/locate/fusengdes

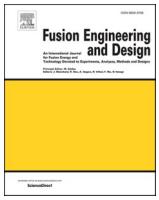

Use of MAXFEA-ANSYS tool to study the Electro-Magnetic behaviour of the new ST40 inner vacuum chamber proposal during a plasma VDE

R. Lombroni [a,*], S. Carusotti [a], F. Giorgetti [a,b], M. Scarpari [a], P.F. Buxton [c], G. Calabrò [a], P. Fanelli [a], M. Romanelli [c], E. Ruiz de Villa Valdes [c], J. Wood [c]

[a] Department of Economy, Engineering, Society and Business Organization (DEIM), University of Tuscia, Largo dell'Università, Viterbo 01100, Italy
[b] Department of Fusion and Nuclear Safety Technology, ENEA, Frascati, Rome 00044, Italy
[c] Tokamak Energy Ltd, 173 Brook Drive, Milton Park, Oxon OX14 4SD, United Kingdom

ARTICLE INFO

Keywords:
MAXFEA code
ANSYS APDL
Tokamak Energy
ST40
Plasma disruptions
VDE
Electro-Magnetic Analysis

ABSTRACT

Tokamak Energy Ltd. is developing compact fusion power plants based on two promising technologies, Spherical Tokamaks (STs) and High Temperature Superconductors (HTS), with the aim to build a first demonstrative plant by the 2030's. On its path to fusion power, Tokamak Energy is presently operating ST40, a new generation ST that is currently the highest field device of its kind. In the near future, an important ST40 upgrade is planned and foresees the manufacturing and the installation of a new vacuum chamber, called IVC2. This upgrade will allow the exploitation of ST40 to its maximum performances enabling Double Null (DN) diverted operations with up to 2 MA of plasma current and 3 T of toroidal field. IVC2 is currently in the final design stage. The necessity to analyse in detail the Electro-Magnetic (EM) behaviour of this component under the loads coming from plasma disruptions has recently emerged in order to verify the design or drive further modifications. In this context, a study to analyse the EM response of IVC2 during a plasma Vertical Displacement Event (VDE) has been carried out using the MAXFEA code in combination with ANSYS APDL, following a recent workflow development. The main output of this study is the evaluation of the transient EM force density in IVC2 and other components for subsequent mechanical assessments. The aim of this paper is to present the results of this analysis to show the successful application of this procedure in the context of ST40 project.

1. Introduction

Tokamak Energy Ltd. is a privately funded company based in the UK. Founded in 2009, the company is developing compact fusion power plants based on two promising technologies: Spherical Tokamaks (STs) and High Temperature Superconductors (HTS) [1–3]. The ST route to fusion has generated considerable interest since the mid-1980s [4–7]. This concept demonstrates all the main feature of high aspect ratio tokamaks having at the same time the potential to significatively reduce costs and timescales on the path to Fusion power. Over the years, research has shown that STs have beneficial properties such as operating at high plasma beta, higher elongation and possibly exhibit higher confinement, although more data are needed at higher field and lower collisionality to determine this fundamental aspect [3]. In the past, the first attempts to design ST based devices did not produce convincing design and until recently STs have remained on the margins of Fusion research. However, recent advances in both tokamak physics and superconductor technology have made a ST fusion reactor a possibility. The key technological advance is the advent of rare-earth HTS. Use of conventional low temperature superconductor (LTS) for a ST device appears in fact impractical because of the thick shielding needed to prevent neutrons heating the superconductor to above 4 K, that is not compatible with the very limited space available in central column of STs. Instead, a HTS magnet can potentially overcome this problem since it can operate at relative high temperatures with less demanding cryogenics (superconductivity occurs at around 91 K in zero magnetic field, but far better performance is achieved when HTSs are cooled to 20 – 40 K [3]). Furthermore, HTSs are able to carry more current at high field, and this allows significant increase in the toroidal field (TF), which was found to improve confinement in STs. The combination of the efficiency of STs and the benefits of the HTS opens a route to lower-volume fusion reactors. The mission of Tokamak Energy is to exploit this opportunity by pioneering the use of spherical tokamaks in conjunction with HTS magnet technology.

* Corresponding author.
E-mail address: riccardo.lombroni@unitus.it (R. Lombroni).

https://doi.org/10.1016/j.fusengdes.2023.113611
Received 21 March 2022; Received in revised form 23 February 2023; Accepted 25 February 2023
Available online 10 March 2023

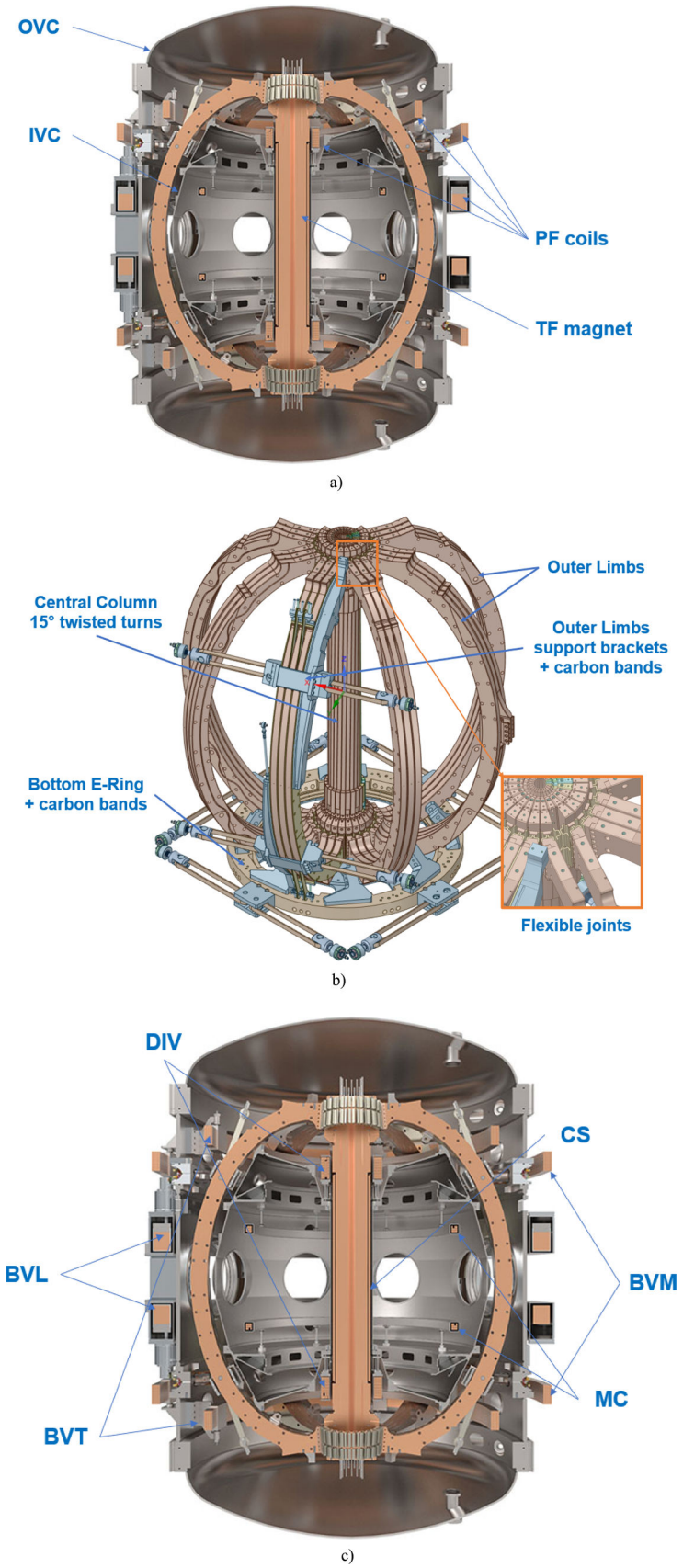

Fig. 1. Overview of ST40 main components a) Poloidal plane view of the main components b) Overview of the TF system with the central column, the outer limbs, the SS brackets + carbon bands, the bottom E-Ring + carbon bands and a zoom of the flexible joint connection c) PF coils system.

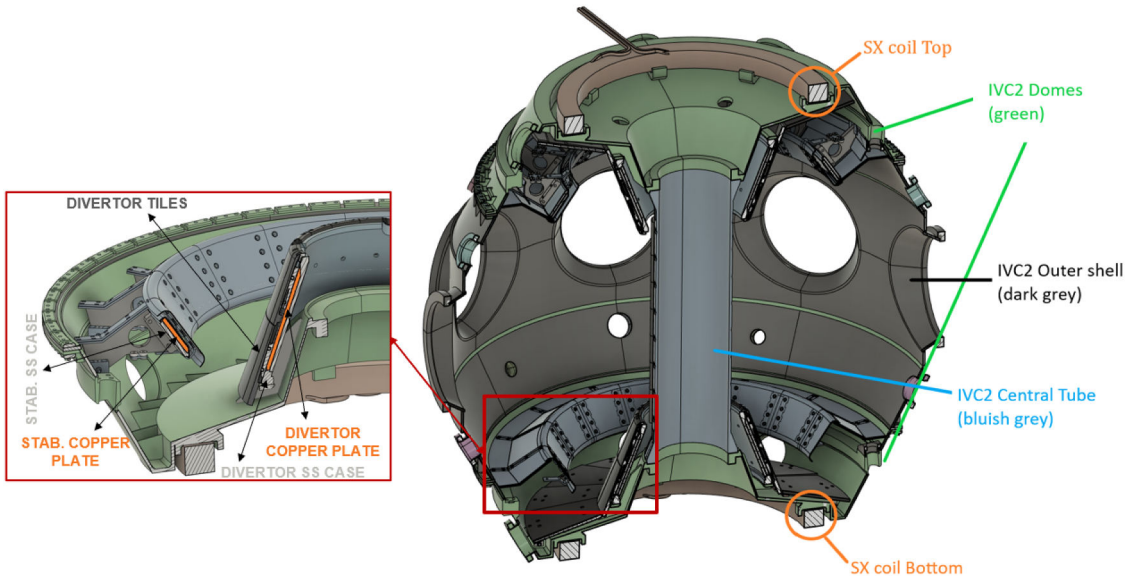

Fig. 2. Overview of IVC2 with the Domes, the Central Tube, the Outer shell and the SX coils with a zoom of the Divertor and the Stabilizing Plate on the left.

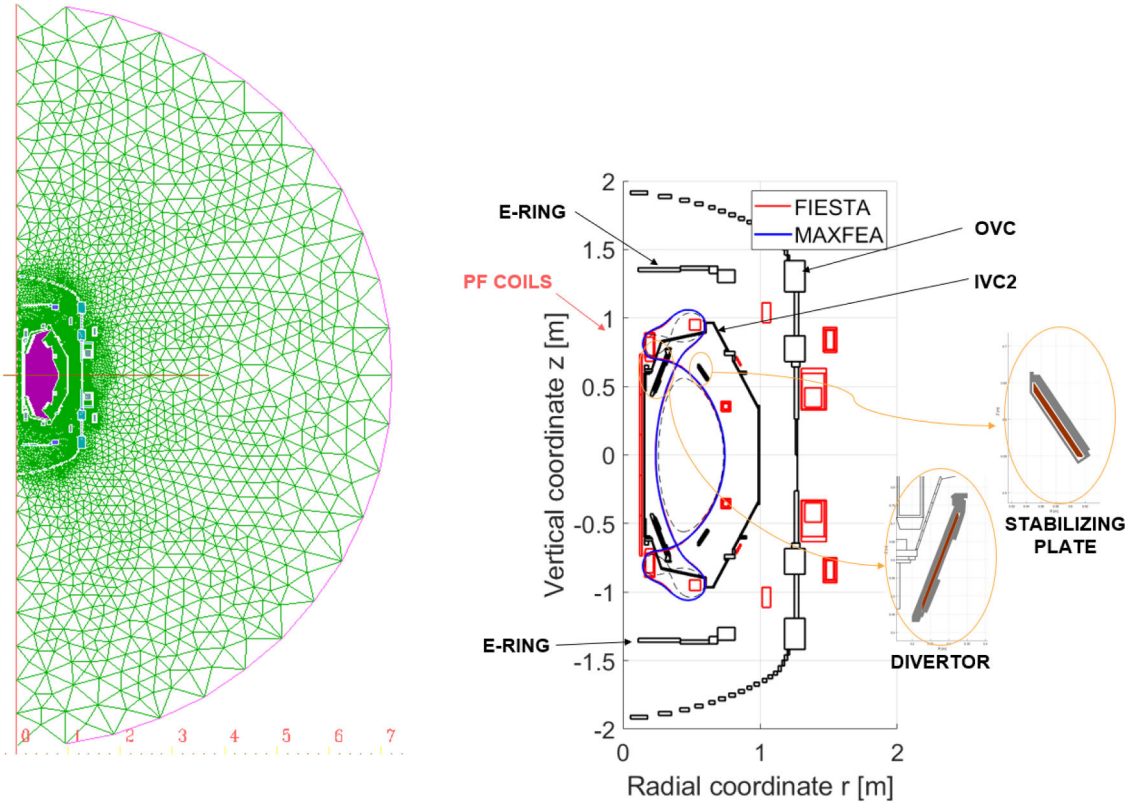

Fig. 3. MAXFEA model (a) Overview of the whole FEM domain (b) Zoom in the plasma region. The PF coils are represented in red. The other components included are indicated with arrows. A zoom of the Divertor and the Stabilizing Plate is shown on the right. The reference equilibrium reproduced by means of MAXFEA is reported in blue, red for FIESTA.

On its path to Fusion power, Tokamak Energy Ltd. is presently operating ST40 [3,8,9]. ST40 is an high field ST whose main design parameters are: $R_0 = 0.4$ - 0.6 m, $A = 1.7$ - 2.0, $I_{PLA} = 2$ MA, $B_T = 3$ T, $\kappa = 2.5$. ST40 is the highest field device of its kind (until recently STs have typically operated at TF around 0.3 – 0.5 T). ST40's main components are presented in Section 2. An overview of ST40's latest experimental results is provided in [10]. In the near future, an important ST40 upgrade is planned and foresees the manufacturing and the installation of a new inner vacuum chamber, called IVC2, that is currently in the final design stage. Therefore, the necessity to analyse in detail the Electro-Magnetic (EM) behaviour of this component under the loads coming from critical EM transients, such as plasma disruptions, has

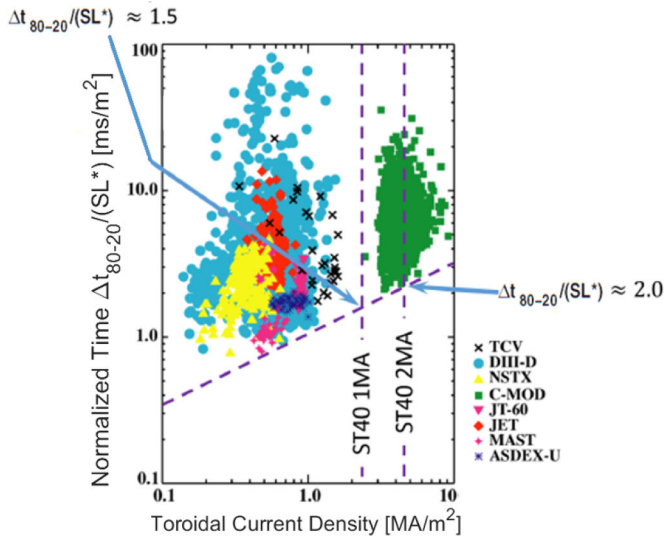

Fig. 4. Statistic distribution of the normalized time $\Delta t_{80-20}/(SL^*)$ versus toroidal current density separated by device with the lower limit assumed for ST40 represented by the dashed line.

Table 1
CQ duration assumption for the simulated scenario (fast UVDE).

Assumption	$\Delta t_{80\text{-}20}/(SL^*) = 2.0$ms m^{-2}
S	0.47 m^2
L*	0.99
Δt_{80-20}	0.9 ms

emerged in order to support/verify the design.

A plasma disruption, often occurring as consequence of transient plasma perturbations [11], is a complex phenomenon involving plasma instabilities which results in a abruptly termination of the plasma and the complete transfer of the plasma thermal and magnetic energy to the surrounding structures on very short timescales, with the potential to inflict severe damages to components. In JET a plasma current of several megaamperes typically decades on a time scale of ~ 5 - 50 ms, resulting in forces of several MN on the vacuum vessel [12]. According to [13], in ITER a maximum vertical force of about 80 - 85 MN is expected during a Vertical Displacement Event (VDE).

The evaluation of the disruptions related effects represent one of the main driver of the design of tokamaks components, to ensure they reach the projected lifetime and fulfil their function even in the worst scenario. Many authors dealt with the study of plasma disruptions effects from both EM and structural points of view. The impacts of plasma disruptions on ITER have been extensively investigated in the last two decades [13–15] using several codes, such as DINA [16] and TSC [17]. EM and structural analyses of disruptions have been carried out also in the context of EAST [18,19] and CFETR [20]. In [21], the authors have recently calculated the DEMO vacuum vessel peak displacements and accelerations during different VDEs. Instead, in [22] a recent overview of the EM methodology applied to support the pre-conceptual design phase of the DEMO Breeding Blanket is provided, with particular emphasis to the EM loads generated during plasma disruptions. So far, preliminary multiphysical analyses were carried out on the DTT machine too, in order to develop the conceptual design of the vacuum vessel [23].

In this paper, the recently developed methodology based on the use of MAXFEA code in combination with ANSYS APDL fully described in [24,25] is used to assess the EM behaviour of IVC2 during plasma disruptions. In particular, the results of a so-called Upward VDE (UVDE) fast disruption are here presented. The main output is the evaluation of

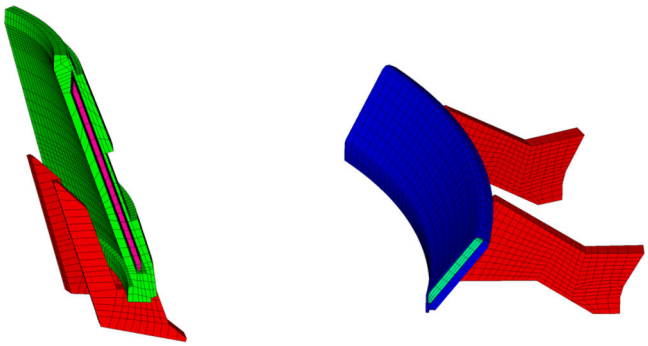

Fig. 6. Zoom of the bottom Divertor (left) and Stabilizing Plate (right).

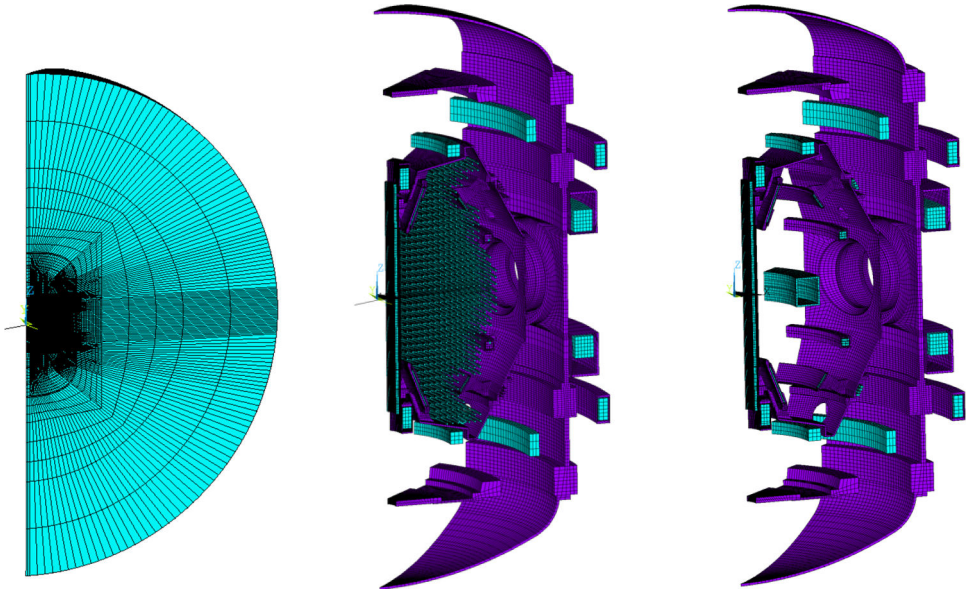

Fig. 5. 3D APDL EM model: overview of the whole model with region (left), mesh with filaments for PFV analysis (centre) and mesh with torus for TFV analysis (right).

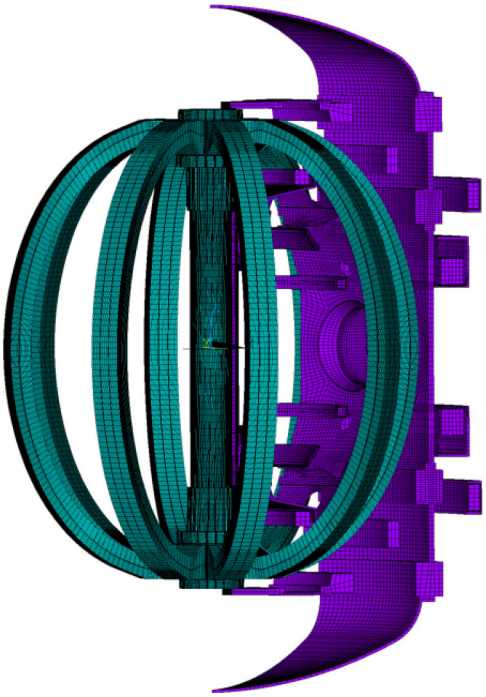

Fig. 7. Overview of the TF COIL MODEL.

the EM force density evolution in the components for subsequent mechanical assessments. In the near future, the models herein developed and the proposed methodology will be used to assess the EM behaviour of IVC2 during other relevant disruption scenarios, exploring parameters space (e.g. different Current Quench (CQ) durations, Thermal Quench (TQ) assumptions, etc.). In fact, different assumptions in the simulations lead to different plasma evolutions, and thus to different local and global currents and forces to be analysed to have a proper verification of IVC2. The scenario herein considered is the first analysed and it is used as example to show the successful application of this methodology in this context.

This paper is the latest in a series of publications regarding the MAXFEA-ANSYS tool. In the previous studies, this methodology has been firstly presented and applicated to DEMO [24], and then used in the context of the DTT project [25]. DEMO was the testbed for the development of the proposed methodology. In particular, [24] presents its application to a simplified model, in which the presence of ferromagnetic in-vessel components such as the breeding blankets and the divertors was neglected. The relative low level of complexity of this first case allowed to test and validate the procedure. Successively, the procedure was used in much more detailed analyses whose main aim was to support the final design of the DTT vacuum vessel. However, some components of DTT were still in a conceptual design phase at that time (e.g. divertor and first wall), therefore they were not represented in details.

Instead, in this study, we have dealt with problems connected with the modelling of a real object, being ST40 an existing device. Here, the main aim is to show the possibility to use this tool when an high level of accuracy in representing the structures is required. Furthermore, since DTT and DEMO can be considered 'conventional' tokamaks, this study aims to demonstrate that this methodology can also be used to support/verify the design of components in advanced non-conventional aspect ratio devices like ST40, showing that its field of application can be extended to this particular class of tokamaks. Indeed, interesting peculiarities of ST40 have emerged and are presented in the paper.

Finally, once the installation of IVC2 is completed, the long-term perspective of our research is to validate the models and the proposed methodology against experimental plasma transients in dedicated experiments, to build confidence in the simulations carried out and, thus, in the IVC2 capability to withstand the loads even in the worst disruption scenarios.

2. ST40 and IVC2

The main components of ST40 are the Inner and Outer Vacuum Chambers (IVC and OVC) and the toroidal and poloidal field (TF and PF) coils [9]. An overview of the current ST40 main components is given in Fig. 1. The OVC is a Stainless Steel (SS) structure that houses the IVC, PF

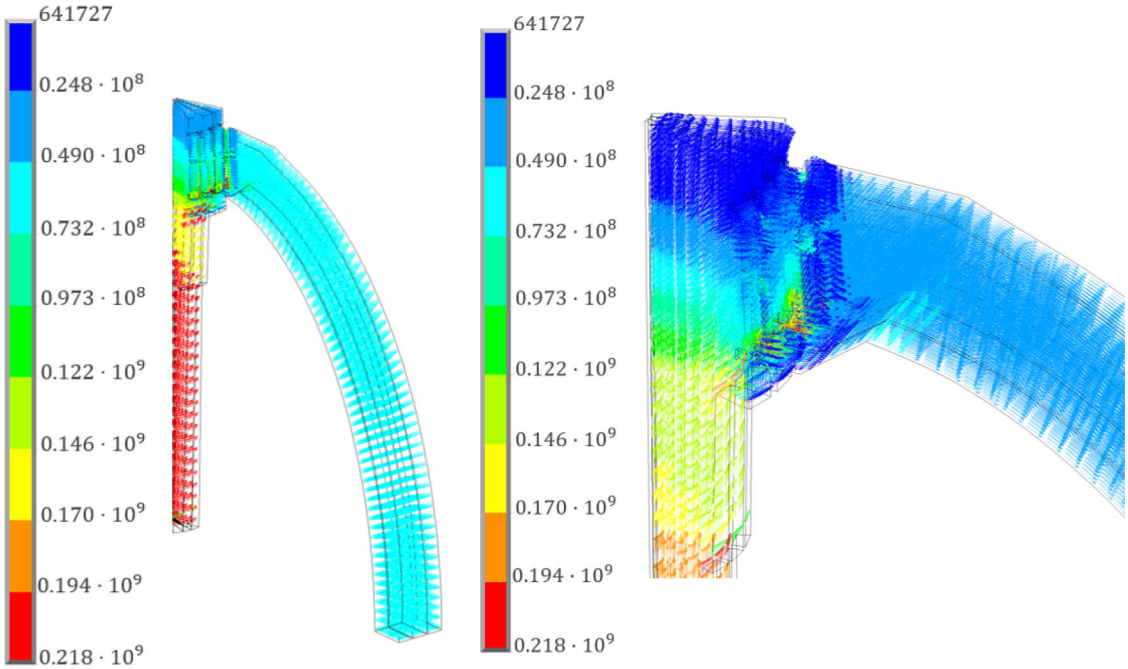

Fig. 8. Current density distribution in the TF coil [A/m^2]. Overview of the upper part of the magnet (left), zoom of the connection between the central column and the outer limb (right).

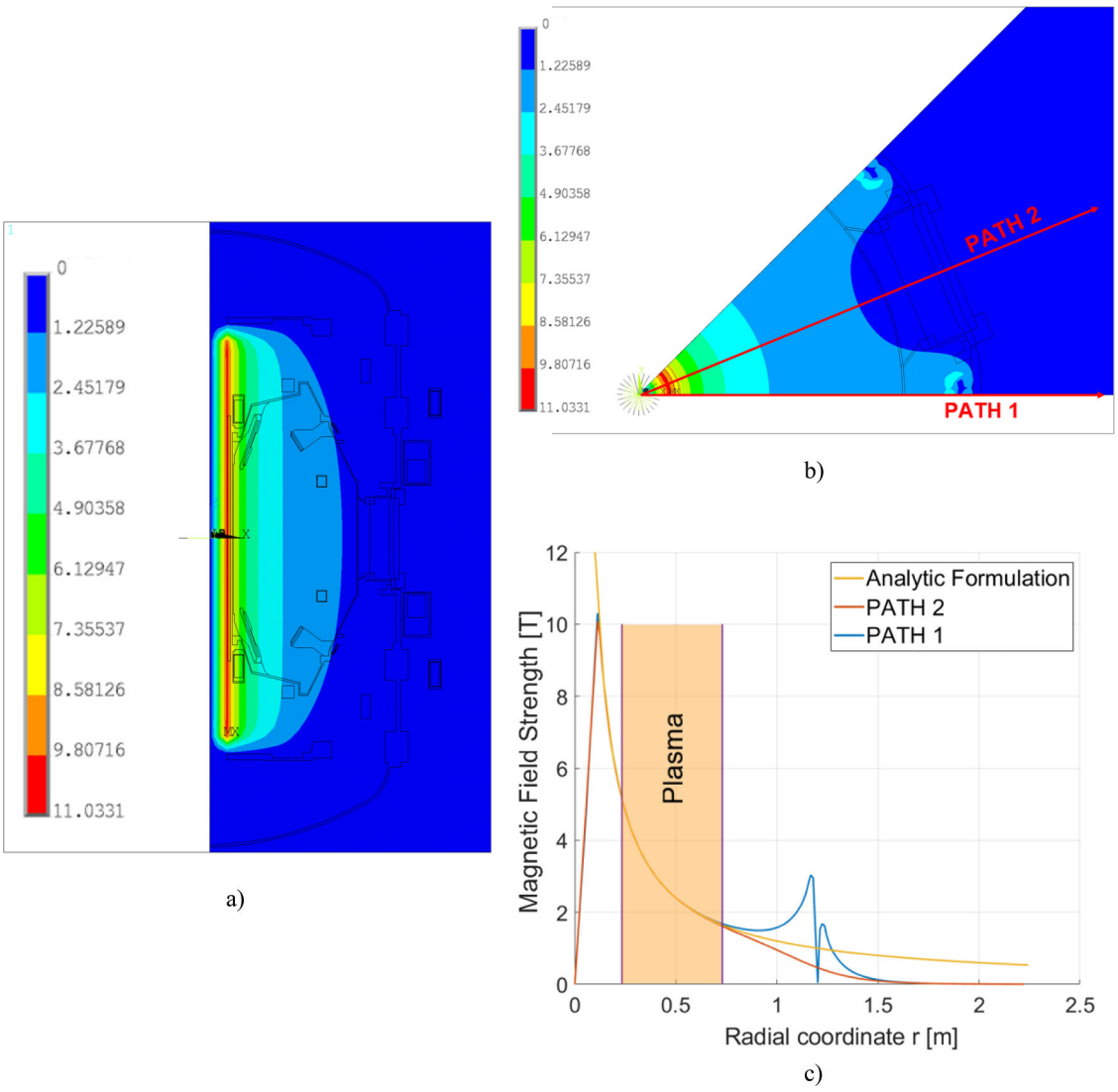

Fig. 9. Magnetic field strength produced by the TF magnet [T] (a) Poloidal Plane (b) Equatorial Plane (c) Magnetic field strength along PATH 1 (blue line) and PATH 2 (red line) together with the analytic formulation (yellow line) $B_T = f/r$, with $f = B_T{\cdot}R = 1.2T{\cdot}m$, where $R = 0.4m$ and $B_T = 3T$.

and TF coils. It has an internal vacuum ($\sim 10^{-2}$ Pa) optimized to provide thermal insulation for the liquid nitrogen-cooled copper coils and to protect from possible electrical breakdowns in the IVC-OVC interspace [9]. The OVC mechanically supports the TF, PF and IVC components and is designed to withstand the EM forces expected during both normal (e.g. TF in-plane and out-of-plane forces, PF forces during the plasma scenario, etc.) and off-normal conditions (i.e. plasma disruptions). It is supported by four legs and the entire assembly sits on top of the assembly platform (not reported Fig. 1). The IVC is made of 10 mm thick 314 SS, apart from the centre tube that is made of 4 mm thick Inconel covered by a set of graphite limiters, and it is designed to be pumped down to $\sim 10^{-6}$ Pa during plasma operation [9]. A couple of up-down symmetric divertors, presenting a castellation of graphite tiles on copper plates and connected with the IVC through SS supports, have recently been introduced in ST40 to enable double null (DN) diverted operations with up to 1MA of plasma current [26].

Regarding the ST40 coils, they are all made of copper. The TF magnet consists of a central column and outer limbs connected together with flexible copper demountable joints. An overview of the TF system is in Fig. 1b. The centre post consists of 24 copper wedges with a 15° twisted in the central part to allow connecting one TF turn to the next, while in the outer zone the turns are arranged in 8 limbs with 3 turns in each. To accommodate the EM forces acting on the magnet, each outer limb is equipped with two SS support brackets (top and bottom), connected to the OVC with two carbon fibre straps each. In addition, there are two torque rings, one at the top and one at the bottom of the device, the so-called E-Rings (see Fig. 1b). These titanium rings add extra support against twisting and are connected to the OVC with eight carbon fibre straps each.

Concerning the PF coils, ST40 presents four pairs of coils, namely the BVL, BVM, BVT and DIV coils, for the plasma current, position and shape control (Fig. 1c). ST40 has also a Central Solenoid (CS) directly wounded on the TF central column to ramp and maintain the flattop current but it is not used for inductive start up. At this end, in fact, ST40 uses a process called merging compression (MC) [27], firstly developed for START [28] and later utilized in MAST [29]. For that purpose, two in-vessel MC coils are installed, as shown in Fig. 1c, together with a pair of push (PSH) coils located outside the IVC.

With the next upgrade, IVC2 will substitute IVC. An overview of IVC2 is reported in Fig. 2 and is composed of three main parts connected through Inconel and SS flanges:

- The domes (top and bottom, green components in Fig. 2), made of Inconel 718
- The outer shell (dark grey component in Fig. 2), made of Inconel 718
- The central tube (bluish grey component in Fig. 2), made of SS316

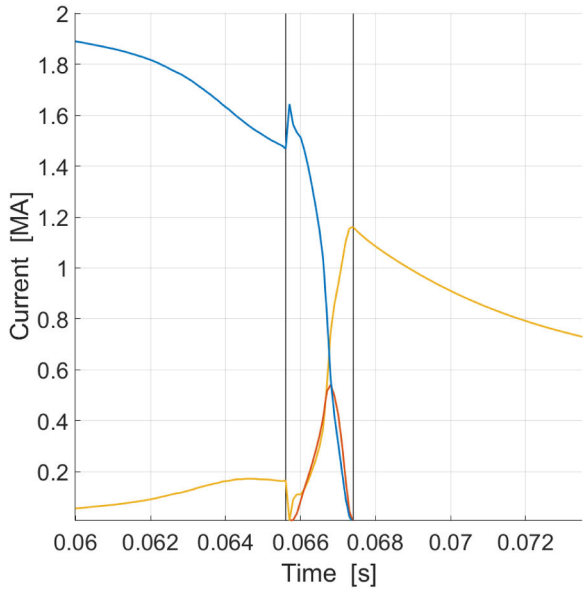

Fig. 10. MAXFEA plasma current (blue curve), eddy currents (yellow curve) and halo currents (red curve).

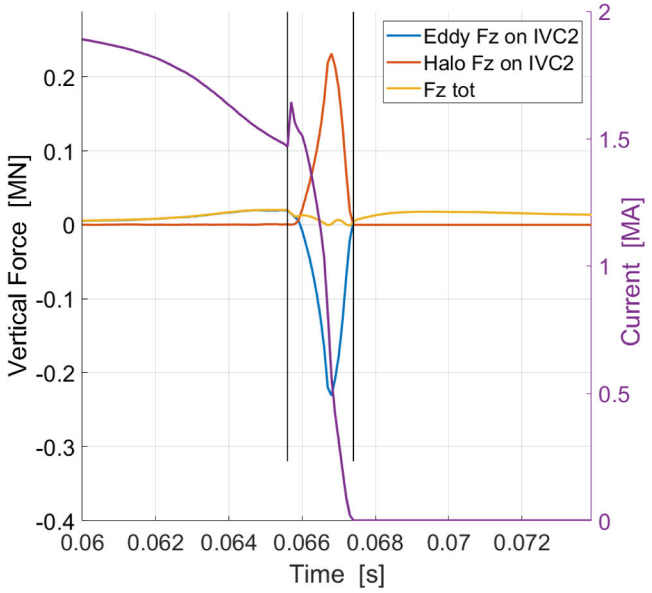

Fig. 11. MAXFEA Vertical Force on IVC2-MS due the eddy currents (blue curve, refers to left ordinate axis), due to the halo currents (red curve, refers to left ordinate axis), due to halo+eddy (yellow curve, refers to left ordinate axis) and plasma current (purple curve, refers to the right ordinate axis).

Together with the IVC2, new divertor and stabilizing plate concepts will be introduced. In particular, two symmetric (top and bottom) divertors will be installed (Fig. 2). The copper stabilization plates will be encapsulated in a SS jacket and connected in anti-series from top to bottom through an interconnection (in this arrangement any up/down symmetric change in flux will not induce any current to flow; but anti-symmetric changes in flux will induce current to flow). A set of molybdenum tiles will be mounted on the SS case and will face the plasma. A similar concept is foreseen for the stabilizing plates. These passive stabilization structures guarantee a significative reduction of the vertical instability growth rate, while allowing for Merging/Compression start up, mid-plane and upper launched NBI's and being compatible with the divertor power exhaust [30].

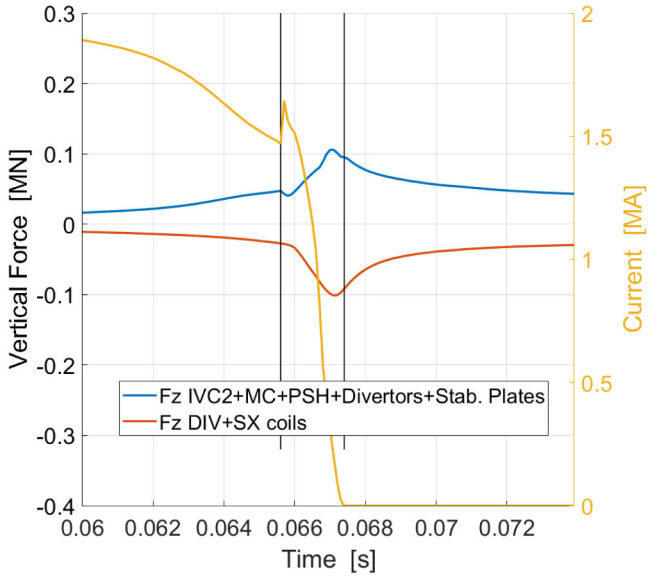

Fig. 12. Vertical force on IVC-MS divided in two sub-components: red curve represents the system composed by DIV and SX coils (refers to left ordinate axis), blues curve represents the system composed by IVC2, MC and PSH coils, Divertors and Stabilizing Plates (refers to left ordinate axis). Plasma current is represented in yellow (refers to right ordinate axis).

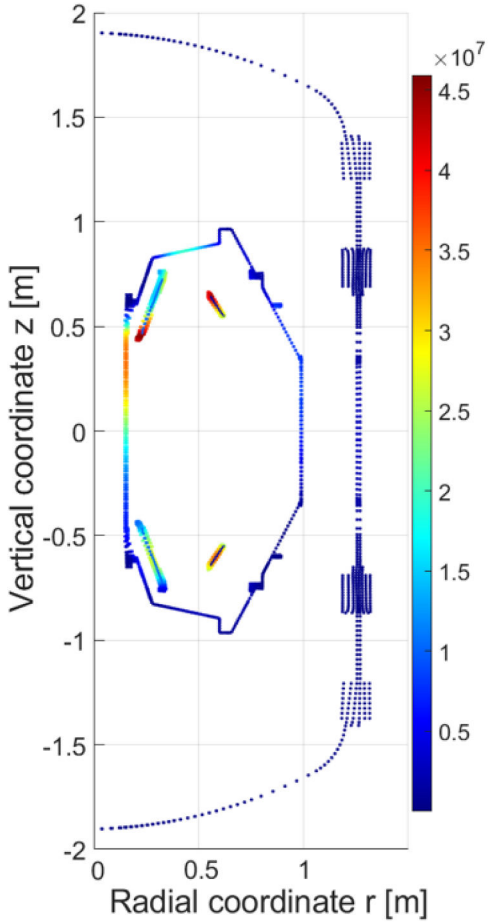

Fig. 13. MAXFEA eddy current distribution [A/m^2] on IVC2 at the end of the CQ (0.0674 s).

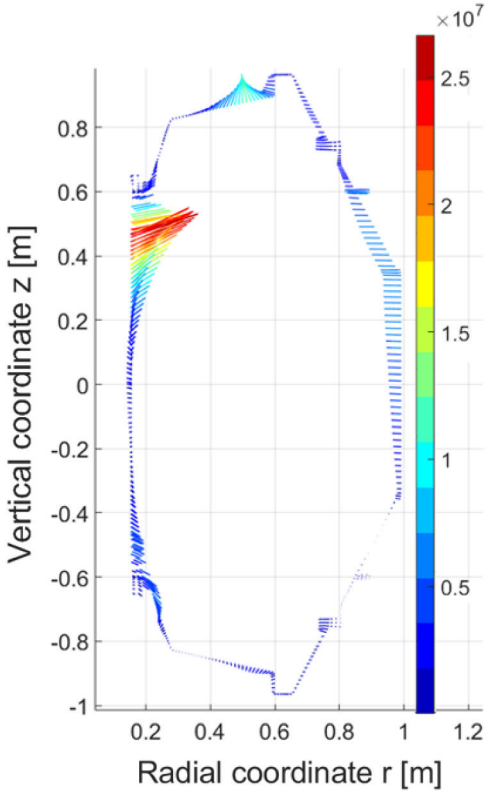

Fig. 14. MAXFEA force density distribution [N/m^3] on IVC2 at the end of the CQ (0.0674 s).

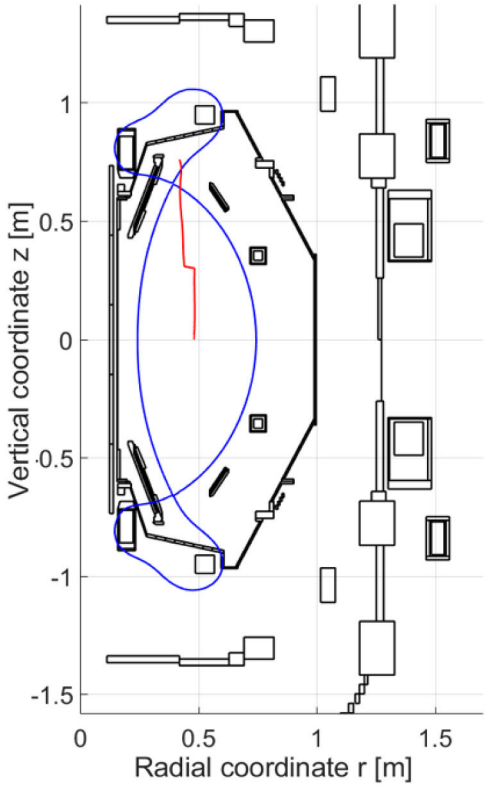

Fig. 15. Initial plasma equilibrium and plasma centroid (RJ-ZJ) movement during the UVDE fast.

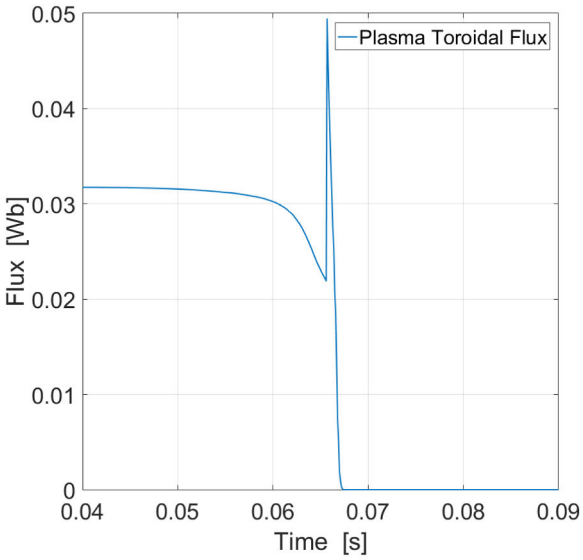

Fig. 16. Plasma TFV evolution during the UVDE.

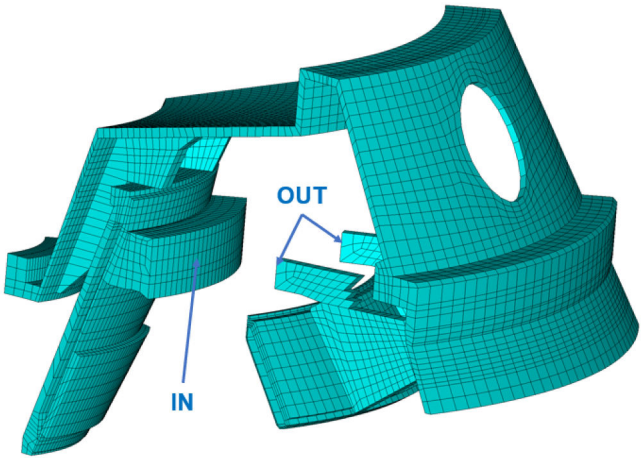

Fig. 17. HC assumed in and out locations.

Furthermore, the upgrade will include the installation of a new set of PF coils, namely the SX coils. These coils will provide for the formation of secondary x-points allowing the test of advanced divertor magnetic configurations, like the reference DN equilibrium analysed in this study and presented in Section 3.1.

In this paper the EM response of ST40 during a plasma UVDE fast is analysed with particular focus on the IVC2 structure. The recently developed procedure based on the use of MAXFEA code in combination with ANSYS APDL (release 20.2) already applied in the context of DEMO [24] and DTT projects [25] has been used to carry out the analysis.

3. FE models

The proposed approach relies on the use of MAXFEA code in combination with ANSYS APDL. Two EM models have been developed, namely the MAXFEA 2D axisymmetric and 3D ANSYS APDL models, together with a separated model of the TF coil developed for a detailed evaluation of the toroidal field on the components.

3.1. MAXFEA 2D axisymmetric model

In this section the MAXFEA model is presented. An overview of the

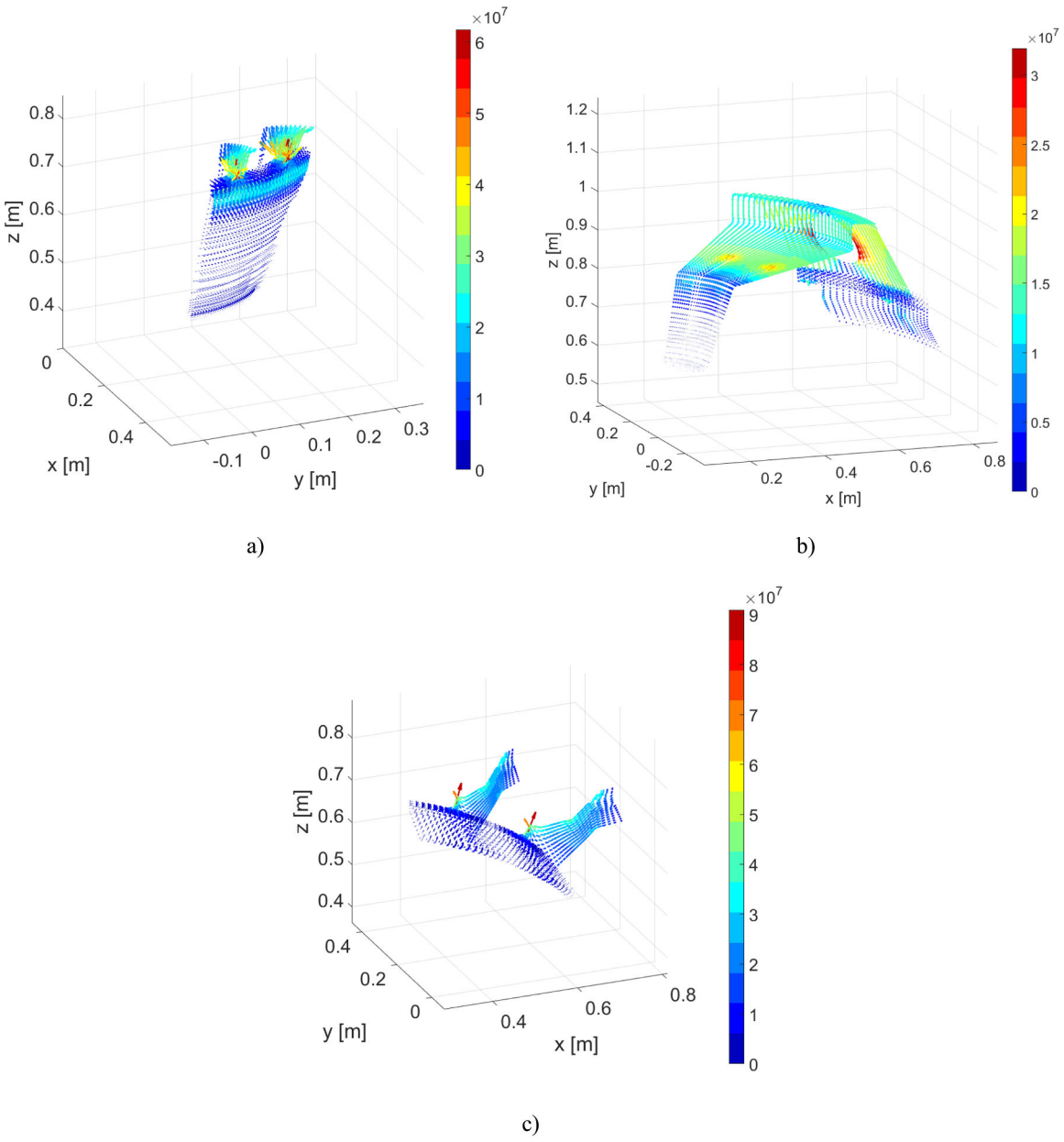

Fig. 18. HC distribution [A/m^2] at its peak (0.0668 s). (x, y, z) are cartesian coordinates. (a) Divertor and supports (b) IVC2 (c) Stabilizing Plate and supports.

model is reported in Fig. 3. The model includes:

- PF coils system (red areas in Fig. 3b):

  In particular, the top and bottom MC coils have been considered connected in series in a closed loop configuration (11 turns each). The same assumption has been made for the PSH coils (8 turns each).

- OVC
- IVC2
- Divertors:

  The toroidal continuous copper plate of the top divertor is connected in anti-series with that of the bottom divertor and they are insulated from the relative SS case.

- Stabilizing Plates:

  The same anti-series connection of the divertors.

- E-Rings

The reference plasma equilibrium reproduced with MAXFEA [31], namely a DN configuration with I_{PLA} = 2 MA, is shown in Fig. 3b, together with that computed by means of FIESTA code. The FIESTA code is a plasma equilibrium code developed in the Culham Centre for Fusion Energy (CCFE) [32]. The comparison shows a very good agreement between the two codes, proving MAXFEA capability to treat such kind of advance plasma configurations.

As far as the disruption scenario is concerned, a fast UVDE has been considered and the following assumptions have been made:

- Destabilizing kick is imposed @ 1 ms after the start of the simulation to force plasma upward movement imposing a small voltage on a dummy coil for few time steps (time step = 0.1 ms).

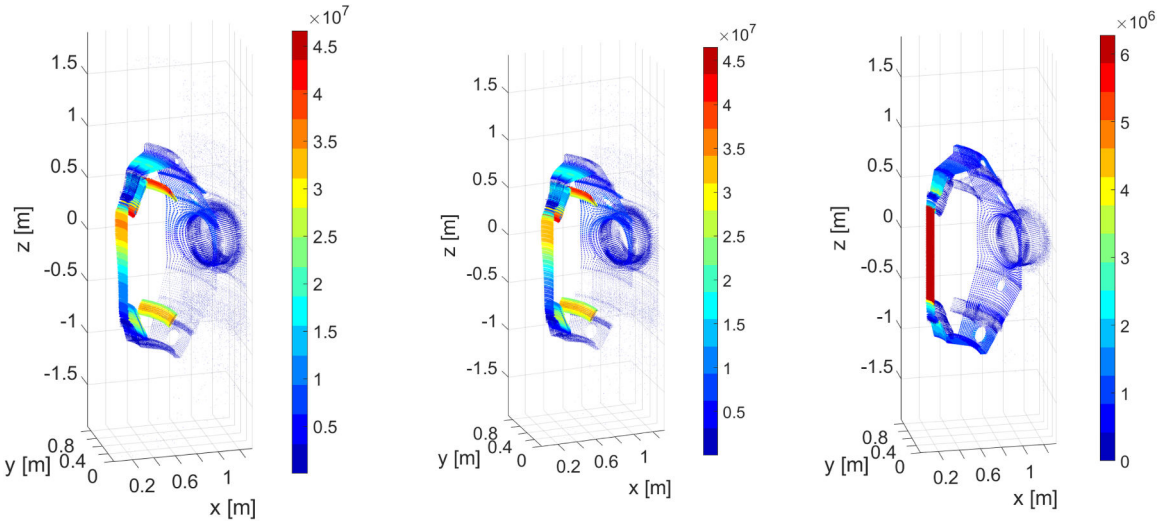

Fig. 19. Eddy current distribution [A/m^2] at the end of the CQ (0.0674 s). (x, y, z) are cartesian coordinates. (a) PFV+TFV (b) only PFV (c) only TFV.

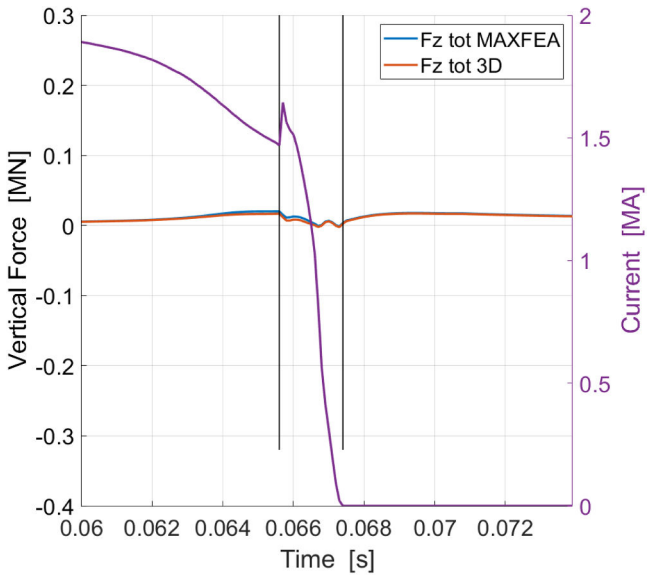

Fig. 20. Comparison of the Total Vertical Force on IVC2-MS: MAXFEA (blue curve, refers to left ordinate axis) vs full 3D analysis (red curve, refers to left ordinate axis). Purple curve represents the plasma current (refers to the right ordinate axis).

- Consequently, the plasma starts to move vertically towards the wall, reducing accordingly the plasma area and the total plasma current since flux conservation is assumed.
- At a certain point, when the plasma touches the wall and becomes limiter, Thermal Quench (TQ) is imposed as a 90% drop in beta poloidal in 1 time step and a plasma current spike is found. This is also regularly observed experimentally, due to the flux conservation and redistribution of the plasma current.
- Current Quench (CQ) starts immediately after, imposing a proper negative voltage on plasma to obtain a desired CQ duration Δt_{cq}. During the CQ phase, halo current growth is considered.

Regarding the CQ assumptions, Δt_{cq} has been evaluated referring to the ITER disruption database (IDDB) [33], that is usually used for characterization of disruptions. Within IDDB, the CQ rate is normalized by the plasma cross-sectional area S and self-inductance L^*, yielding to the normalized time $\Delta t_{cqSL} = \Delta t_{80\text{-}20}/(SL^*)$, where $\Delta t_{80\text{-}20} = t_{80} - t_{20}$ is typically used to derive the linear CQ rate. In particular, t_{80} and t_{20} are the times when the plasma current reaches 80% and 20% of its pre-disruptive value, respectively (see [33] for further details). Fig. 4 shows the normalized time Δt_{cqSL} distribution versus the toroidal current density j_p separated by device. This definition allows to better compare CQ rates of different devices and place a lower bound on the fastest expected Δt_{cq}. Specifically, since ST40 operates in range of high j_p, $\Delta t_{80\text{–}20}$ has been calculated according to what shows in Fig. 4 and Table 1, yielding to $\Delta t_{80\text{–}20} = 0.9$ ms.

3.2. APDL 3D models

The 3D APDL model is shown in Fig. 5. The model consists of a ST40 sector (45°) and features approximately 850 thousand elements and 700 thousand nodes. The adopted element type is the SOLID97 that features up to 4 Degree of Freedom (DoF), namely the three vector potential A components (for all conductive and non-conductive elements) and the VOLT (for current induction). The model features an high quality mapped mesh, with a mean values in terms of skewness and warping factor of about 0.220 and 0.004, respectively. Only 0.617% and 0.045% of the elements exceed skewness > 0.7 and warping factor > 0.3, respectively, and it is worth to say that these elements are localized in very limited zone of the air domain, far enough from the region of interest.

The same mesh model is adopted for Poloidal Field Variation (PFV), Toroidal Field Variation (TFV) and Halo Current simulations (HC). In this way, the various EM contributions can be easily added element by element, facilitating post-processing operations. Following the methodology presented in [24,25] the plasma PFV is simulated by means of set of filaments (Fig. 5 centre), whilst the plasma TFV is reproduced via a thin torus onto which an equivalent poloidal current is applied (Fig. 5 right). Regarding the HC simulation, the total HC computed with the MAXFEA simulation is injected into the structures through chosen in and out locations. The assumption of the in and out locations will be presented in Section 4.3. The adopted Boundary Conditions (BCs) depend on the simulation considered, but in any case, have the capability to reproduce the symmetry of the system. Fig. 6 shows a zoom of the Divertor and the Stabilizing Plate.

To simplify the whole model and reduce significatively its dimension, the presence of the TF coil system is neglected, since its presence does not affect the results significatively. The contribute of the magnetic field produced by the TF magnet on the structures is evaluated with a magnetostatic analysis by means of a different dedicated model (herein identified as TF COIL MODEL). The developed model is shown in Fig. 7.

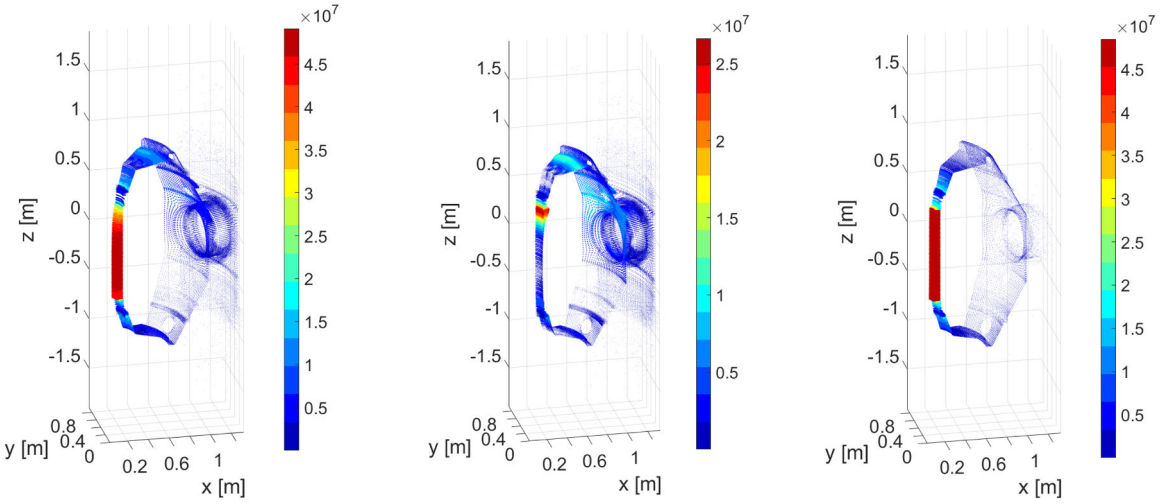

Fig. 21. Force density distribution [N/m^3] at the end of CQ (eddy current peak, 0.0674). (x, y, z) are cartesian coordinates. (a) PFV+TFV (b) only PFV (c) only TFV.

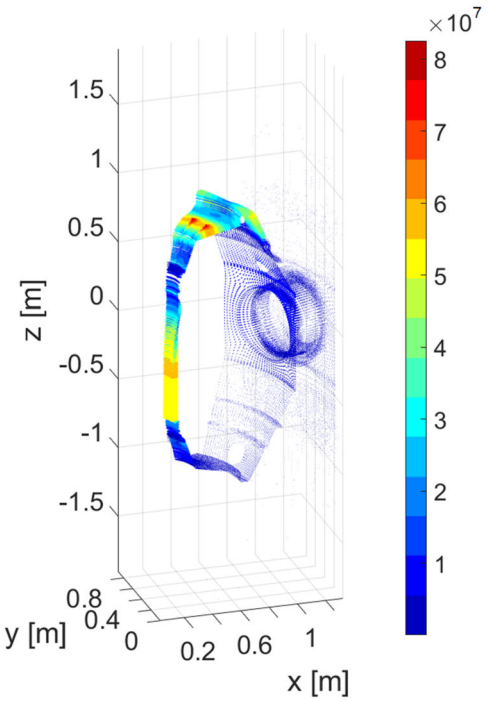

Fig. 22. Force density distribution [N/m^3] at the HC peak (0.0668 s). (x, y, z) are cartesian coordinates.

It consists in a full detailed 360° mesh of the TF magnet with the 15° twisted central wires, the outer limbs and the flexible joint connections. The adopted element type is SOLID5 which allows the computation of the magnetic field in the components by means of an integral formulation. Therefore, no air mesh is required. The TF model features approximately 1.1 million elements and 1.4 million nodes. Computing the toroidal field with this level of detail allows us to evaluate the effect of the ripple and the presence of possible local effects due to the close vicinity of certain components with the magnet turns.

4. Results

4.1. TF coil magnetostatic analysis

As discussed, the contribution of the magnetic field produced by the TF magnet on the structures is evaluated with a magnetostatic analysis by means of the TF COIL MODEL. Fig. 8 shows the current density distribution in the TF turns together with a zoom corresponding to the connection between the central column and the outer limb, and Fig. 9a-b show the resulting magnetic field strength in the poloidal and equatorial planes, respectively. From Fig. 9b, it is possible to observe the presence of the ripple. In Fig. 9c, the magnetic field strength along PATH 1 and PATH 2 (shown in Fig. 9b) is reported together with the simplified analytic formulation of the field as $B_T = f/r$, with $f = B_T R = 1.2T\ m$, where $R = 0.4\ m$ and $B_T = 3\ T$. From this Fig., we see the ripple has a negligible effect within the plasma zone.

4.2. MAXFEA analysis

The results of the MAXFEA simulation are reported from Fig. 10 to Fig. 16. Fig. 10 shows the plasma current evolution (named I_{pla} and depicted with blue curve). In an initial phase of the scenario, when the plasma is moving upward before it touches the wall, a current reduction is observed because of the flux conservation assumption. At a certain point the plasma touches the wall. In correspondence of this time instant, that takes place at 0.0656 s and it is identified with left black vertical line in Fig. 10, TQ is imposed and a current spike is found due to the sudden redistribution of the plasma current. CQ takes place immediately after and ends at 0.0674 s (identified with right black vertical line). In the CQ phase, HC arises as shown with the red curve, reaching a peak of about 0.54 MA at 0.0668 s. At the end of this phase, at 0.0674 s, eddy current reaches its maximum of about 1.18 MA (yellow curve).

The vertical EM forces acting on the IVC2 are instead reported in Fig. 11. The total vertical force acting on the IVC2 due to the eddy currents is represented in blue (note that this is the result of the interaction between toroidal eddy currents and poloidal field, since MAXFEA assumes axisymmetry). This force is equal to the sum of the force directly experienced by the IVC2 and the forces that act on the components that are mechanical connected to it, namely the DIV, SX, PSH and MC coils, the Divertors and the Stabilizing Plates. It should be intended as the resultant force experienced by the OVC. This sub-system of components, in fact, is mechanically connected with the OVC by means of a set of gravity supports (in the remainder of the paper, this sub-system will be named IVC2-MS). This force shows a peak of about −0.23 MN at 0.0668 s. Similarly, the red curve - that represents the global vertical force due to the halo current – shows a peak of about 0.23 MN occurring at the same time instant. The fact that these two curves present a similar behaviour is an interesting result connected with the peculiarities of ST40. Unlike conventional devices like ITER, DEMO [24] or DTT [25], in which the system composed by the vacuum vessel and

the in-vessel components is mechanically independent from the one composed by external coils, in ST40 some of the PF coils are mechanical connected with IVC2.

This circumstance, together with the up and down symmetry of the machine and of the external currents, produces a compensation effect in the global force acting on the IVC2-MS. In particular, the force remains small during the CQ as shown by the yellow curve in Fig. 11 (sum of the red and blue curves). It is possible to better understand this fact observing Fig. 12, where the global force on IVC2-MS is divided in two sub-components. As shown, the force acting on the DIV and SX coils produces a compensation effect that attenuates the resultant force on the IVC2-MS gravity supports.

In Figs. 13 and 14 the current density and force distributions in the IVC2 at the end of the CQ (0.0674 s) are shown, respectively. In Fig. 15 the evolution of the plasma current centroid (R_J - Z_J) during the UVDE together with the initial plasma equilibrium (blue curve) is reported. Fig. 16 shows the plasma TFV flux evolution in time.

4.3. 3D analysis

Downstream the MAXFEA simulation, 3D EM analyses have been carried out introducing the plasma evolution in the 3D model with the methodology exposed in [24,25]. In the next figures, a cartesian system of coordinates with the origin located at the machine centre is used (machine centre is the point located at (0,0) in Fig. 3b). Regarding the HC, the assumed in and out locations are shown in Fig. 17. The HC is injected into the Divertor Case and flows towards the IVC2 through the Divertor support. Once in IVC2, the HC circulates in clock-wise direction from the Divertor to the Stabilizing Plate. Finally, it reconnects through the Stabilizing Plate supports and comes back to the plasma. Fig. 18a shows the HC distribution in the Divertor and its supports at 0.0668 s, when HC is at its maximum. Instead, in Fig. 18b the HC distribution in IVC2 at the same time instant is presented, whilst Fig. 18c shows the HC in the Stabilizing Plate and its supports.

As far as the eddy current from PFV and TFV is concerned, Fig. 19a provides an overview of the current density distribution in IVC2 at the end of the CQ (0.0674 s), when eddy current reaches its maximum. The PFV and TFV contributions are reported separately in Fig. 19b and Fig. 19c, respectively. As it emerges from Fig. 19c, the current from TFV flow mostly poloidal in clockwise direction reaching a peak in the central tube of about 6.2 MA/m^2. Instead, eddy current from PFV flows mostly in toroidal direction presenting a peak of about 46 MA/m^2 in the upper Divertor and Stabilizing Plate, one order of magnitude higher than the peak observed for the TFV.

A comparison in terms of vertical force between MAXFEA and 3D analyses is shown in Fig. 20. Instead, Figs. 21 and 22 present force density distributions on IVC2 at two different time: at the eddy current peak (Fig. 21), at 0.0674 s (end of CQ), and at the HC peak (Fig. 22), at 0.0668 s. These forces comprehend all the EM contributions (PFV+TFV+HC), including the toroidal field coming from the magnetostatic analysis. The results highlight that the presence of the 3D structures (e.g. ports, Divertors and Stabilizing Plates supports, etc.) does not strongly affect the IVC2-MS response in terms of global force, that remains approximately the same during the CQ. However, if 3D effects are considered, a non-trivial distribution of forces arises, generating local concentrations not evaluable in MAXFEA. In particular, from Fig. 21a, it emerges that the zone of highest loads is localized the central tube (~50 MN/m^3). Here, the force is mainly directed radially inboard and it is principally due to the interaction between the poloidal current coming from the TFV and the toroidal field. This means that this kind of interaction is predominant with respect to the forces due to the interaction between the toroidal current coming from the PFV and the poloidal field, which are the main responsible of the net vertical force. This is an interesting result connected with the peculiarities of ST40. In fact, in conventional devices like ITER, DEMO [24] or DTT [25], the opposite usually happens. Here, this particular behaviour is connected to the close vicinity of the inboard part of the vacuum vessel to the magnet central column, which results in an intense toroidal field. This effect can be better appreciated in Fig. 21c that shows the force density distributions related to the eddy from TFV only. Fig. 21b reports instead the isolated contribution of the eddy from PFV.

When the HC reaches its peak, at 0.0668 s, another zone of high force concentration emerges in the upper part of IVC2 (Fig. 22). Here, the force density is mainly orientated in vertical direction and it is dominated by the interaction between the HC and the toroidal field, reaching a peak of about 80 MN/m^3 in correspondence of the Divertor supports connections. In the central tube it is possible to observe the behaviour discussed before, but the force concentration is less intense here since the eddy current is lower than at the end of the CQ.

5. Conclusions

In this paper, the recently developed methodology based on the use of MAXFEA code in combination with ANSYS APDL fully described in [24,25] has been applied to evaluate the EM behaviour of IVC2 during a plasma disruption. In particular, an Upward VDE (UVDE) fast disruption has been considered. Differently from the previous papers of this series [24,25], in this study we have dealt with problems connected with the modelling of a real object, showing the possibility to use this tool when an high level of accuracy in representing the structures is required. Moreover, this study aimed to demonstrate the possibility to use this methodology to support/verify the design of components in advanced non-conventional aspect ratio devices like ST40.

Interesting results have emerged from this analysis. It has been found that the total vertical force on IVC2-MS remains small during the disruption. This result is connected with the peculiarities of ST40. In fact, unlike conventional devices like ITER, DEMO [24] or DTT [25], in which the system composed by the vacuum vessel and the in-vessel components is mechanically independent from the one composed by external coils, in ST40 some of the PF coils are mechanical connected with IVC2. This circumstance, together with the up and down symmetry of the machine and of the external currents, determines a compensation effect that contributes to attenuates the resultant force on the gravity supports. Nevertheless, this does not mean that individual components are not interested by intense loads. Indeed, high force distributions have been found on IVC2. In particular, it emerged that the highest peaks in the eddy current related force density are concentrated in the inboard part of IVC2 as consequence of the interaction of the poloidal current due to the TFV and the toroidal field (~ 50 MN/m^3 at the end of CQ). This kind of interaction, not evaluable in MAXFEA, proved to be predominant with respect to the forces due to the interaction between the toroidal current from the PFV and the poloidal field. This interesting result was found to be connected with the peculiarities of ST40 of having the inner part of the vacuum vessel in close vicinity with the magnet central column, which results in an intense toroidal magnetic field. Instead, when the HC reaches its peak, it has emerged that the highest load in the IVC2 occurs in correspondence of the Divertor supports connections in the upper part of IVC2 (~ 80 MN/m^3). Here, the force density is mainly orientated in vertical direction and it is dominated by the interaction between the HC and the toroidal field. Also in this case this force distribution, not evaluable in MAXFEA, is too relevant to be neglected. Conversely, in terms of global forces, MAXFEA and 3D analyses highlight comparable results, showing that the main component of the force that determines net resultants in the components is connected to the interaction of the toroidal current from PFV and the poloidal field.

The long-term perspective of this research is to validate the models and the proposed methodology against experimental plasma transients in dedicated future experiments, to build confidence in the simulations carried out and, thus, in the IVC2 capability to withstand the loads even in the worst disruption scenarios.

CRediT authorship contribution statement

R. Lombroni: Conceptualization, Methodology, Software, Validation, Formal analysis, Investigation, Data curation, Writing – original draft, Writing – review & editing, Visualization. **S. Carusotti:** Software, Validation, Formal analysis, Data curation, Writing – review & editing, Visualization. **F. Giorgetti:** Conceptualization, Methodology, Software, Validation, Formal analysis, Writing – review & editing, Visualization. **M. Scarpari:** Software, Validation, Formal analysis, Data curation, Writing – review & editing, Visualization. **P.F. Buxton:** Conceptualization, Resources, Writing – review & editing, Supervision, Project administration, Funding acquisition. **G. Calabrò:** Conceptualization, Resources, Writing – review & editing, Supervision, Project administration, Funding acquisition. **P. Fanelli:** Conceptualization, Resources, Writing – review & editing, Supervision, Project administration, Funding acquisition. **M. Romanelli:** Conceptualization, Resources, Writing – review & editing, Supervision, Project administration, Funding acquisition. **E. Ruiz de Villa Valdes:** Conceptualization, Resources, Writing – review & editing, Supervision. **J. Wood:** Software, Validation, Formal analysis, Writing – review & editing.

Declaration of Competing Interest

The authors declare that they have no known competing financial interests or personal relationships that could have appeared to influence the work reported in this paper.

Data availability

The data that has been used is confidential.

References

[1] https://www.tokamakenergy.co.uk/(accessed Feb 17, 2022).
[2] McNamara, Steven, and Tokamak Energy Team. 'Tokamak energy and the high-field spherical tokamak route to fusion power.' APS Division of Plasma Physics Meeting Abstracts. Vol. 2019. 2019.
[3] A. Sykes, et al., Compact fusion energy based on the spherical tokamak, Nucl. Fusion 58 (1) (2018).
[4] M. Ono, R. Kaita, Recent progress on spherical torus research, Phys. Plasmas 22 (4) (2015).
[5] Y.K.M. Peng, D.J. Strickler, Features of spherical torus plasmas, Nucl. Fusion 26 (6) (1986) 769–777.
[6] A. Sykes, Spherical tokamak programme at Culham, Nucl. Fusion 39 (1999) 1271–1281. Special Issue.
[7] J.E. Menard, et al., Fusion nuclear science facilities and pilot plants based on the spherical tokamak, Nucl. Fusion 56 (10) (2016).
[8] M. Gryaznevich, Faster fusion: ST40, engineering, commissioning, first results, AIP Conf. Proc. 2179 (2019). November.
[9] M. Gryaznevich, O. Asunta, Overview and status of construction of ST40, Fusion Eng. Des. 123 (2017) 177–180.
[10] McNamara, Steven, Overview of recent results from the ST40 high-field spherical tokamak, Bull. Am. Phys. Soc. 66 (2021).
[11] G. Sias, et al., Inter-machine plasma perturbation studies in EU-DEMO relevant scenarios: lessons learnt for EM forces prediction during VDEs, Nucl. Fusion (2022). Feb.
[12] F.C. Schuller, Disruptions in tokamaks, Plasma Phys. Control. Fusion 37 (11A) (1995).
[13] M. Sugihara, et al., Disruption scenarios, their mitigation and operation window in ITER, Nucl. Fusion 47 (4) (2007) 337–352.
[14] S. Miyamoto, et al., Simulation of VDE under intervention of vertical stability control and vertical electromagnetic force on the ITER vacuum vessel, Fusion Eng. Des. 87 (11) (2012) 1816–1827.
[15] S. Miyamoto, et al., Inter-code comparison benchmark between DINA and TSC for ITER disruption modelling, Nucl. Fusion 54 (8) (2014), 083002. Aug.
[16] R.R. Khayrutdinov, V.E. Lukash, Studies of plasma equilibrium and transport in a tokamak fusion device with the inverse-variable technique, J. Comput. Phys. 109 (2) (1993) 193–201. Dec.
[17] S... Jardin, N. Pomphrey, J. Delucia, Dynamic modeling of transport and positional control of tokamaks, J. Comput. Phys. 66 (2) (1986) 481–507. Oct.
[18] W. Xu, X. Liu, Y. Song, J. Li, M. Lu, Electromagnetic and structural analyses of the vacuum vessel and plasma facing components for EAST, Fusion Eng. Des. 88 (9–10) (2013) 1848–1852.
[19] L. Sumei, S. Jinxin, L. Mingxuan, L. Mingzhun, P. Kun, Electromagnetic and structure analysis for EAST vacuum vessel with plasma facing components during VDE, Fusion Eng. Des. 124 (2017) 410–414.
[20] S. Liu, M. Chen, M. Lei, M. Lu, Z. Wang, Electromagnetic and structural analysis on vacuum vessel for CFETR during plasma major disruption, J. Fusion Energy 33 (6) (2014) 713–719.
[21] F. Giorgetti, et al., Dynamic behaviour of DEMO vacuum vessel during plasma vertical displacement events, Fusion Eng. Des. (2020).
[22] I.A. Maione, et al., Electromagnetic analysis activities in support of the breeding blanket during the DEMO pre-conceptual design phase: methodology and main results, Fusion Eng. Des. 166 (2021) no. February.
[23] E. Martelli, et al., Design status of the vacuum vessel of DTT facility, Fusion Eng. Des. 172 (2021), 112760. Nov.
[24] R. Lombroni, F. Giorgetti, G. Calabrò, P. Fanelli, G. Ramogida, Using MAXFEA code in combination with ANSYS APDL for the simulation of plasma disruption events on EU DEMO, Fusion Eng. Des. 170 (March) (2021), 112697. Sep.
[25] F. Giorgetti, et al., Vertical displacement events analysis using MAXFEA code in combination with ANSYS APDL in the final design stage of the DTT vacuum vessel, Fusion Eng. Des. 184 (August) (2022), 113273. Nov.
[26] Romanelli, Michele, Integrated modelling of plasmas in the ST40 high-field spherical tokamak, Bull. Am. Phys. Soc. 66 (2021).
[27] P. Buxton, et al., Merging compression start-up in ST40, P1, 047, in: Proceedings of the 29thSymposium on Fusion Technology (SOFT 2016), 2016.
[28] A. Sykes, et al., First results from the START experiment, Nucl. Fusion 32 (4) (1992) 694–699.
[29] A. Sykes, et al., First results from MAST, Nucl. Fusion 41 (10) (2001) 1423–1433.
[30] P.F. Buxton, et al., On the design and role of passive stabilisation within the ST40 spherical tokamak, Plasma Phys. Control. Fusion 60 (6) (2018).
[31] P. Barabaschi, The MAXFEA code, Proc. Plasma Control, Technical Meeting (Naka, Japan, April 1993)".
[32] G. Cunningham, Fiesta training course presentation. CCFE, 2013.
[33] N.W. Eidietis, et al., The ITPA disruption database, Nucl. Fusion 55 (6) (2015) 63030.